Atmos. Chem. Phys. Discuss., 14, 3777–3814, 2014
www.atmos-chem-phys-discuss.net/14/3777/2014/
doi:10.5194/acpd-14-3777-2014

Atmospheric Chemistry and Physics Discussions

Climatology of aerosol optical properties and black carbon mass absorption cross section at a remote high altitude site in the Western Mediterranean Basin

M. Pandolfi, A. Ripoll, X. Querol, and A. Alastuey

Institute of Environmental Assessment and Water Research (IDAEA-CSIC), Barcelona, Spain

Received: 3 December 2013 – Accepted: 31 January 2014 – Published: 11 February 2014

Correspondence to: M. Pandolfi (marco.pandolfi@idaea.csic.es)

Published by Copernicus Publications on behalf of the European Geosciences Union.

Abstract

Aerosol light scattering, backscattering and absorption were measured at Montsec (MSC; 42°3′ N, 0°44′ E, 1570 m a.s.l.), a remote high-altitude site in the Western Mediterranean Basin. Mean (±sd) scattering, hemispheric backscattering and absorption were $18.9 \pm 20.8\,Mm^{-1}$, $2.6 \pm 2.8\,Mm^{-1}$ and $1.5 \pm 1.4\,Mm^{-1}$, respectively at 635 nm during the period under study (June 2011–June 2013). Mean values of single scattering albedo (635 nm), scattering Ångström exponent (450–635 nm), backscatter-to-scatter ratio (635 nm), asymmetry parameter (635 nm) and black carbon mass absorption cross section (637 nm) were 0.92 ± 0.03, 1.56 ± 0.88, 0.16 ± 0.09, 0.53 ± 0.16 and $10.9 \pm 3.5\,m^2\,g^{-1}$ respectively. The scattering measurements performed at MSC locate this site in the medium/upper range of values reported for other mountaintop sites in Europe mainly due to the frequent African dust episodes and regional recirculation scenarios occurring mostly in spring/summer and causing the presence of polluted layers at the MSC altitude. Under these conditions no clear diurnal cycles were observed for the measured extensive aerosol optical properties (scattering, absorption and extinction). Conversely, the mean particle absorption at MSC was relatively lower compared with other EU remote stations thus leading to relatively higher single scattering albedo compared with most European data. A season-dependent decrease in the magnitude of aerosol extensive properties was observed when MSC was in the free troposphere with the highest *free-troposphere* vs. *all-data* difference observed in winter and the lowest in spring/summer. The slope of the scattering vs. absorption relationship (among the lowest reported for other mountain top sites worldwide) indicates that the MSC site is dominated by dust aerosols at high aerosol loading. Correspondingly, scattering Ångström exponent and asymmetry parameter respectively decreased and increased indicating the shift toward larger particles associated with African dust episodes. The black carbon mass absorption cross section showed a clear annual cycle with higher values in summer when the occurrence of African dust outbreaks and regional recirculation scenarios favour the presence of aged black carbon particles in polluted layers at

ACPD
14, 3777–3814, 2014

the MSC altitudes. The optical measurements performed at the MSC remote site were compared with those simultaneously performed at a regional background station in the Western Mediterranean Basin.

1 Introduction

Atmospheric aerosols affect the Earth's radiative balance directly, by scattering and absorbing solar and terrestrial radiation, and indirectly, by acting as cloud condensation nuclei, thus modifying the physical and optical properties of clouds. The measurements of aerosol optical properties such as scattering, backscattering, absorption, and extinction are important for aerosol characterization and model validation and, consequently, for a better comprehension of the role of aerosols in the Earth-atmosphere system (IPCC, 2007, 2013). Specific aerosol optical parameters such as single scattering albedo (SSA), scattering Ångström exponent (SAE), backscatter-to-scatter ratio (B/S), asymmetry parameter (g), black carbon (BC) mass absorption cross section (MAC), among others, can be derived from these optical properties. The cooling or absorbing potential of atmospheric aerosols mostly depends on these parameters which are complex function of aerosols size, shape, chemical composition and refractive index. The majority of particles scatter the sun light causing a net cooling at the top of the atmosphere (TOA), whereas soot particles (or BC) have strong absorbing properties over the entire visible spectrum which lead to a net warming of the Earth-atmosphere system (IPCC, 2007, 2013). BC particles play a role second only to carbon dioxide in climate change and are co-emitted with a variety of other aerosols and precursor gases which can increase the light absorption by BC through an increase in its MAC (e.g. Bond et al., 2013). Given that atmospheric models convert the modelled/measured BC mass concentrations to optical absorption using the MAC, accurate estimates of MAC values and of the possible reasons explaining their variability are important.

Aerosol optical measurements are carried out worldwide by both in-situ and remote techniques. In order to address the uncertainties related with the geographical varia-

ACPD
14, 3777–3814, 2014

tion in aerosols optical properties, networks such as ACTRIS (Aerosols, Clouds, and Trace gases Research InfraStructure Network; www.actris.net) or the NOAA's baseline observatory (http://www.esrl.noaa.gov/gmd/) were created. The ACTRIS network aims at integrating three existing European research infrastructures: EUSAAR (European Supersites for Atmospheric Aerosol Research; for in-situ aerosol measurements at regional level; http://www.eusaar.net), EARLINET (European Aerosol Research Lidar Network, for remote aerosol measurements; http://www.earlinet.org) and CLOUDNET (to provide a systematic evaluation of clouds in forecast models, http://www.met.rdg.ac.uk/radar/cloudnet/). Thus, the ACTRIS project provides the unique opportunity to integrate in-situ and vertical aerosol measurements for the characterization of both the planetary boundary layer (PBL) and the free troposphere (FT). The measurements of aerosols in the FT are especially important given that FT aerosols are more spatially representative of the global atmosphere than the aerosols in the PBL due to their long residence time (of the order of several weeks). Aerosols in the FT can be transported over long distances and have extended climate and air quality impacts (Laj et al., 2009; Andrews et al., 2011). Due to the location of the majority of the in-situ ACTRIS stations, the in-situ measurements are performed mainly within the PBL whereas the vertical lidar measurements allow for aerosol optical measurements almost in the whole troposphere. However, lidars do not measure key climate variables such as aerosol absorption, SSA or MAC and the in-situ measurements (which provide these key variables) are often limited to the PBL. Consequently, the measurements performed at mountaintop observatories provide the opportunity to make long-term, continuous observations of in-situ aerosol properties in the free troposphere (FT). Moreover, given their frequent position in the FT, mountaintop stations give the possibility to study aerosols under different atmospheric scenarios without strong interference from closer anthropogenic emissions. However, the number of mountaintop observatories providing long-term in-situ aerosol optical measurements worldwide is rather low. Recently, Andrews et al. (2011) presented climatologies for free tropospheric aerosol radiative properties utilizing in-situ data from ten high altitude stations in the 20–50° N

ACPD
14, 3777–3814, 2014

latitude band. Examples of high altitude aerosol optical measurements were presented by Bodhaine (1983, 1995), Delene and Ogren (2002), McKendry et al. (2011), Marcq et al. (2010), Collaud Coen et al. (2004, 2007, 2011), Cozic et al. (2008), Andrews et al. (2004, 2011), Marinoni et al. (2008), Nyeki et al. (1998).

In this work we present the results from two year measurements (June 2011–June 2013) of aerosol optical properties performed at the high altitude Montsec station (MSC) which is run following the ACTRIS standards. Data from MSC were compared with data collected at the ACTRIS Montseny station (MSY, 41°19′ N, 02°21′ E, 720 m a.s.l.): a regional background (RB) station located around 140 km East from MSC. Seasonal and diurnal variation of extensive (scattering, absorption, extinction) and intensive (SSA, SAE, B/S, and g) aerosol properties and of BC MAC are presented and discussed. The effects of four main season-dependent synoptic atmospheric scenarios affecting the Western Mediterranean Basin (WMB) on the measured optical properties are also discussed. Moreover, the data collected when the MSC station is in the FT are compared with the free tropospheric aerosol optical properties presented in Andrews et al. (2011) for other mountaintop sites.

2 Measurement site and methodology

2.1 Montsec measurement station

The MSC site (42°3′ N, 0°44′ E, 1570 m a.s.l.) is a high altitude emplacement located in the NE of the Iberian Peninsula (Fig. 1) and situated in the southern side of the Pre-Pyrenees at the top of the Montsec d'Ares mountain. This region is low-density populated and isolated from large pollutant emissions, 140 km from the highly urbanized and industrialized coastline to the SE, 30 km from the largest city around the region (Balaguer, 15 769 inhabitants) to the S, and 50 km from the axial Pyrenees to the N. The ACTRIS RB station of MSY is located around 140 km from MSC site.

ACPD
14, 3777–3814, 2014

Aerosol measurements presented in this work were performed at MSC during the period June 2011–June 2013. Due to the deployment of the nephelometer in measurement campaigns at other locations, scattering and backscattering data were not available from Feburary 2012 to June 2012. Results from MSC site were compared with those simultaneously obtained at the RB MSY station (Fig. 1). A description of the MSY site and of the optical measurement performed at MSY can be found in Pandolfi et al. (2011).

2.2 Optical measurements

2.2.1 Scattering, hemispheric backscattering and absorption

Particles scattering (σ_{sp}; 0–360°) and hemispheric backscattering (σ_{bsp}: 90°–270° coefficients at three wavelengths (450 nm, 525 nm, 635 nm) were measured with a LED-based integrating nephelometer (model Aurora 3000, ECOTECH Pty, Ltd, Knoxfield, Australia). All acronyms used in this work are reported in Table 1. The σ_{sp} and σ_{bsp} data were corrected for truncation errors and for non-ideal (non-Lambertian) illumination function of the light source as described by Müller et al. (2011a). Müller et al. (2011a) provided parameterized correction factors for each wavelength as linear relationship of the Ångström exponents calculated from uncorrected multi-wavelength scattering measurements. A full calibration of the nephelometer was performed four times per year by using CO_2 as span gas while zero measurements and adjusts were performed once per week by using internally filtered particle free air.

In order to reduce the effects of hygroscopicity enhancing the scattering properties of particles, a relative humidity (RH) threshold of 40 % was set in the sampling cell by using a processor-controlled automatic heater inside the nephelometer. This experimental procedure, which follows the ACTRIS standards, was applied elsewhere (see for example Pereira et al., 2011; Anderson and Ogren, 1998; Pandolfi et al., 2011). The mean RH in the nephelometer sampling cell during the study period was 28.4 ± 9.5 %. Moreover, in-cloud data were removed by selecting only those data with ambient RH < 90 %.

ACPD
14, 3777–3814, 2014

The detection limits of Aurora 3000 over one minute averaging time are 0.11, 0.14, 0.12 Mm^{-1} for total scattering at 450, 525, and 635 nm, respectively, and 0.12, 0.11, 0.13 Mm^{-1} for backscattering (Müller et al., 2011a).

Aerosol absorption coefficients (σ_{ap}) at 637 nm (Müller et al., 2011b) were measured with Multi Angle Absorption Photometers (MAAP, model 5012, Thermo). The detection limit of the MAAP instrument is lower than 0.6 Mm^{-1} over 2 min integration. Absorption measurements are converted by the MAAP's software in BC concentration (in $\mu g\,m^{-3}$) assuming a constant MAC of 6.6 $m^2\,g^{-1}$ (Petzold et al., 2004).

The nephelometer and MAAP instruments were connected to two separated sampling lines with cut-off diameters of 2.5 µm and 10 µm, respectively and placed at about 1.5 m above the roof of the cabin hosting the instruments. The inlets flow was 1 $m^3\,h^{-1}$ and humidity control was performed by connecting a drier to the sampling inlet. The Reynolds number for the described inlet was around 1300. The scattering, backscattering and absorption measurements reported in this work were adjusted to standard temperature and pressure (STP, $T_{standard}$ = 273.15 K and $P_{standard}$ = 1013.25).

2.2.2 PM measurements

Real time PM_{10}, $PM_{2.5}$ and PM_1 mass concentrations were continuously measured, on an hourly base, by using a GRIMM optical counter (model 1107). Subsequently, the PM_x concentrations were corrected with factors obtained by comparing the real time and simultaneous in situ gravimetric measurements (Querol et al., 2008). PM_x gravimetric measurements on a 24 h base were performed twice per week with high volume (Hi-Vol) samplers (DIGITEL and MCV at 30 $m^3\,h^{-1}$) with appropriate PM_x cut-off inlets.

2.2.3 EC measurements

The sampled 24 h filters from Hi-Vol were analysed by means of a SUNSET OCEC analyzer for the determination of elemental carbon (EC) concentrations. The EUSAAR 2

ACPD
14, 3777–3814, 2014

protocol (Cavalli et al., 2010) was used. In this work the uncertainties for the measured EC concentrations were calculated by adding one half of the minimum measured EC concentration to the 7 % of the concentrations (Err[EC] = min[EC]/2 + 0.1 · [EC]). With the EUSAAR 2 protocol the EC uncertainties have been estimated around 2–7 % (JRC report, 2009). The formula applied here gives higher uncertainty to low EC concentrations (e.g. Polissar et al., 1998).

2.3 Data processing

In this work the aerosol scattering, backscattering and absorption coefficients were integrated over 1 h. Five additional parameters (B/S, g, SSA, SAE and BC MAC) were derived starting from the performed optical measurements. The B/S parameter, which is the ratio between hemispherical backscatter and total scatter, is used here to estimate the g of airborne particles used in radiative transfer calculations (Andrews et al., 2006). Values of g can range from −1 for 180° backwards scattering to +1 for complete forward scattering (0°), with a value of 0.7 commonly used in radiative transfer models (Ogren et al., 2006). Following Delene and Ogren (2002) and Andrews et al. (2006), g was calculated for the three nephelometer wavelengths as it follows:

$$g = -7.14(B/S)^3 + 7.46(B/S)^2 - 3.96(B/S) + 0.9893 \quad (1)$$

The SSA indicates the relative amounts of radiation scattered and absorbed by particles. Thus, SSA is a parameter indicating the potential for aerosols for cooling or warming the atmosphere. It is defined as:

$$\mathrm{SSA} = \frac{\sigma_{\mathrm{sp}}}{\sigma_{\mathrm{sp}} + \sigma_{\mathrm{ap}}} \quad (2)$$

Non-absorbing particles such as sulfate have an SSA of one (cooling) while lower SSA values indicate the presence of more absorbing particles. BC particles have an SSA of about 0.2 (warming). In this work SSA was estimated at 635 nm.

ACPD
14, 3777–3814, 2014

The SAE was calculated from the multiwavelenghts nephelometer data as:

$$\mathrm{SAE} = -\frac{\log\left(\sigma_{\mathrm{sp}}^{\lambda_1}/\sigma_{\mathrm{sp}}^{\lambda_2}\right)}{\log\left(\lambda_1/\lambda_2\right)} \quad (3)$$

The SAE describes the λ-dependence of particle scattering coefficient. An Ångström exponent of 4 represents the scattering from molecules (Rayleigh's regime). A large SAE (higher than 2) implies scattering dominated by submicron particles, while SAE values lower than one represent an aerosol distribution dominated by coarser particles (e.g. Schuster et al., 2006). The 450 and 635 nm wavelengths were used for the calculation of SAE.

Given the position of MSC station often in the free troposphere, the B/S, g, SSA and SAE parameters were estimated by using only data (scattering, hemispheric backscattering and absorption) above detection limit (DL) of the instruments.

The BC MAC was estimated from error-weighted linear fitting between σ_{ap} from MAAP and EC concentrations from off-line filter analysis. MAAP data were averaged over the filter sampling time.

2.4 Main meteorological patterns

In order to determine and classify the atmospheric episodes affecting MSC, HYSPLIT (http://ready.arl.noaa.gov/HYSPLITtraj.php), BSC/DREAM8b (http://www.bsc.es/projects/earthscience/DREAM), SKIRON (http://forecast.uoa.gr/dustindx.php) and NAAPS (http://www.nrlmry.navy.mil/aerosol) models were used. 120 h backward trajectories (for 12 p.m. modeling vertical velocity and for 3 different heights, 750, 1500 and 2500 m a.g.l.) were computed for each day of measurements, and classified according to their predominant transport direction in: (1) Atlantic Ocean (AA; Atlantic North and Atlantic North-West; 52 %), (2) North Africa (NAF; 14 %), (3) Winter Regional (WREG, from November to April; 6 %), and (4) Summer Regional (SREG, from May to October; 9 %). The global atmospheric circulation has some seasonal oscillations, thus

ACPD
14, 3777–3814, 2014

MSC is more westerly and northerly influenced in winter, while in summer the prevailing winds come from the South (Ripoll et al., 2013). Consequently, AA episodes are more frequent in winter, whereas continental NAF air masses are more frequent in summer (Pandolfi et al., 2011; Querol et al., 2009; Pey et al., 2009; Pérez et al., 2008; Rodríguez et al., 2001). The advection of clean Atlantic air masses during the cold season clears out the previously accumulated pollution in the aged air masses, leading to lower pollutant concentrations. In summer the meteorology of the area is mainly characterized by long dry periods, sporadic but occasionally heavy rains, and a prevalence of NAF outbreaks (Rodriguez et al., 2004). The WREG and SREG scenarios represent mainly air masses from the Iberian Peninsula (IP) (Rodriguez et al., 2004). In winter (WREG) recurrent anticyclonic conditions with weak synoptic winds lead to stagnation of air masses and to the accumulation and aging of pollutants over the region. Under these conditions the planetary boundary layer (PBL) height mostly determines the dilution of pollutants around the emission sources and the degree of pollution at more elevated/regional areas in the WMB (e.g. Jorba et al., 2013). In summer, due to the intense and rapid solar heating of the lower atmospheric layers, convergence of surface winds from the coast to the central IP plateau injects polluted air into the middle troposphere up to 3.5–5 km (Millán et al., 1997; Pérez et al., 2004). This pattern allows the recirculation and accumulation of aerosol and has the potential to form stratified reservoir layers of aged pollutants which subside over the coastal area and the sea (e.g. Millán et al., 1992; Gangoiti et al., 2001; Pérez et al., 2004).

3 Results and discussion

3.1 General features

Figure 2 shows the temporal series of aerosol components and parameters measured at MSC from June 2011 to June 2013. Nephelometer data were not available from Feburary 2012 to June 2012. The statistics for these parameters, including means,

ACPD
14, 3777–3814, 2014

standard deviations, percentiles (1, 10, 25, 50, 75, 99 percentiles), minima and maxima values and skewness are reported in Table 2. The skewness measures the degree of asymmetry of a distribution function with positive/negative skewness leading to frequency distributions with tails toward values higher/lower than the mean. Thus, the distribution is skewed to the right if skewness > 0 or skewed to the left if skewness < 0. Normal distributions are symmetrical with a skewness of 0. All parameters showed skewness higher than 1 with the exception of SAE and MAC, for which almost normal distributions (skewness close to zero) were observed, and SSA and g both showing a negative skewness. A negative skewness indicates that values lower than the mean are more probable than values higher than the mean. Similar SSA skewness was presented from Pandolfi et al. (2011) at the MSY RB measurement site. Negative skewness for g is a consequence of the high positive skewness observed for B/S.

Hourly σ_{sp} and σ_{bsp} at 635 nm at MSC ranged between 0.1 and 161.1 Mm^{-1} (mean (±sd): 18.9 ± 20.8 Mm^{-1}) and between 0.0 and 17.1 Mm^{-1} (mean: 2.6 ± 2.8 Mm^{-1}), respectively. Mean values of σ_{sp} and σ_{bsp} at 450 nm and 525 nm are reported in Table 2. The σ_{ap} (at 637 nm) ranged between about 0.0 and 12.6 Mm^{-1} with a mean value (of 1.5 ± 1.4 Mm^{-1}. The Hourly PM_1 levels at MSC ranged between about 0.1 $\mu g\,m^{-3}$ and 49.9 $\mu g\,m^{-3}$ with mean value of 5.3 ± 4.5 $\mu g\,m^{-3}$.

As shown later the lowest scattering, backscattering and absorption at MSC were measured under AA and WREG episodes typically observed during the cold season in the WMB. Conversely, high σ_{sp}, σ_{bsp} and σ_{ap} were measured during NAF and SREG episodes.

A comparison between measurements performed at MSC with those reported for other high altitude sites is reported in the following of this text and in the next paragraphs. At the Jungfraujoch high alpine site (3580 m a.s.l.), Fierz-Schmidhauser et al. (2010) reported mean σ_{sp} at 550 nm of about 12 Mm^{-1}, by excluding NAF episodes, and around 20 Mm^{-1}, considering only the NAF episodes. At Izaña (Canari Island, ~ 2400 km a.s.l.) mean σ_{sp} and σ_{ap} at 550 nm of about 10 Mm^{-1} and 0.8 Mm^{-1},

ACPD
14, 3777–3814, 2014

respectively, have been measured (Andrews et al., 2011). In Italy (Monte Cimone, ~ 2200 m a.s.l.) Andrews et al. (2011) reported mean σ_{sp} and σ_{ap} of around 11 Mm^{-1} and 3 Mm^{-1}, respectively. The values measured at MSC were lower compared with the values reported by Pandolfi et al. (2011) for the RB MSY station. Mean σ_{sp} (635 nm) and σ_{ap} (637 nm) at MSY were around 26.6 Mm^{-1} and 2.8 Mm^{-1}, due to the higher influence of anthropogenic emissions at regional level (MSY) compared with remote level (MSC).

The mean B/S (525 nm), SAE (450–635 nm), SSA (635 nm) and g (525) measured at MSC were 0.13 ± 0.07, 1.56 ± 0.88, 0.92 ± 0.03 and 0.59 ± 0.13, respectively. These values were very close to the values reported for the alpine Jungfraujoch site (Fierz-Schmidhauser et al., 2010) indicating similarities in the mean aerosol characteristics observed at these two stations. The main difference was observed for SAE which value was slightly higher at Jungfraujoch (1.671–1.787) compared with MSC (1.56) indicating the prevalence of slightly coarser aerosols at MSC, probably due to the difference in intensity and frequency of NAF episodes between the two sites, with MSC site more affected. At the regional background station of MSY mean B/S, SAE and SSA of 0.135, 1.33 and 0.90, respectively, were measured.

The mean MAC (±sd) at MSC was around 11 ± 2 $m^2 g^{-1}$ and ranged from 2.4 to 20.8 $m^2 g^{-1}$. As shown later (paragraph 3.5) the MAC at MSC showed a clear seasonal dependence. The MAC can change as a function of aerosol composition and age, and therefore it can differ depending on the area under study and the meteorological scenarios. MAC between 7 $m^2 g^{-1}$ and 20 $m^2 g^{-1}$ have been often reported in literature (e.g. Quinn and Bates, 2005; Bond and Bergstrom, 2006; Fernandez-Camacho et al., 2010; Arnott et al., 2003, 2005; Reche et al., 2011; Pandolfi et al., 2011; Querol et al., 2013).

ACPD
14, 3777–3814, 2014

3.2 Diurnal cycles and cluster analysis

As shown in Fig. 3 the mean scattering and absorption at MSC showed diurnal cycles (DC) with lower values at night and higher values in the afternoon. Thus, on average, thermally driven upslope winds and PBL height oscillations favour the transport of pollutants toward the MSC site during the warmest hours of the day. The absolute values of extensive optical properties and PM mass concentrations and their DC amplitudes were higher at MSY RB site compared with MSC (Fig. 3). The lower altitude of MSY site (720 m a.s.l.) and its proximity to anthropogenic pollutant emissions (~ 40 km from Barcelona Metropolitan Area and coastline; Fig. 1) compared to MSC, make more effective the pollution potential of thermally-driven atmospheric processes such as the upslope winds and PBL oscillations. As a consequence the SSA and SAE at MSY station showed marked DC compared with MSC due to the effectiveness of the transport of fine highly absorbing particles of anthropogenic origin at RB sites (Fig. 3).

The σ_{sp} and σ_{ap} measured at MSC showed marked differences as a function of the considered synoptic scenarios with the lowest values measured under AA and WREG scenarios and the highest measured under NAF and SREG (Fig. 3). The mean scattering at MSC under NAF and SREG scenarios were close to the values measured at the RB MSY station, whereas lower scattering was measured at MSC under AA and WREG compared to MSY. Similar pattern was observed for fine PM_1 concentrations (Fig. 3). The similarities in σ_{sp} between MSC and MSY under NAF and SREG demonstrate the potential of these two atmospheric scenarios in polluting both regional and remote areas in the WMB. The potential of SREG scenarios to produce atmospheric reservoir layers of aged pollutants is demonstrated also by the similarity in the concentrations of fine PM at both sites despite their different altitude and distance from important pollution sources (Fig. 3). Conversely, mean σ_{sp} and PM_1 concentrations at MSC under WREG were relatively lower compared to MSY despite the general winter antyciclonic conditions in the WMB which favour the accumulation of pollutants around the emission sources. However, as already stated, the degree of pollution at more

ACPD
14, 3777–3814, 2014

rural/remote/elevated areas under WREG strongly depends on PBL height. The absorption measured at MSC was lower compared with MSY for all considered scenarios as a consequence the proximity of MSY station to important BC anthropogenic sources (cities and industrialized/urbanized coastline) compared with MSC. As a consequence, the SSA was higher at MSC than at MSY irrespective of the atmospheric scenarios. The highest SSA at both sites was measured under NAF scenarios due to the higher relative concentrations of dust particles from Africa enhancing the scattering. Finally, the SAE showed similar characteristics at the two sites with lower values observed under NAF (due to the transport of coarser particles) and higher values under SREG (due to the increased relative concentration in the atmosphere of fine (PM_1) particles of anthropogenic origin).

3.3 FT vs. all data

For the identification of *FT data* we followed the definition given by Andrews et al. (2011; AND2011 from now on) based on the use of data collected between 3 and 09:00 LT. As reported in AND2011, this criterion appears to be reasonable for most mountaintop sites and seasons. The limitations of this "time of day" approach are related with the location, height and topography of the site which determine the strength and frequency of local thermally-driven flow and the presence/intensity of polluted residual layers. All these factors make it difficult to rigorously define FT air. In the WMB the frequent SREG and NAF episodes in spring/summer further complicate the identification of this FT air. Figure 4 shows the mean values for all period (June 2011–June 2013) and by season at MSC for the six aerosol optical parameters presented in AND2011. MSC data were scaled to a wavelength of 550 nm (used in AND2011) by using 1.6 as SAE (median values for MSC; this work) and 1 as absorption Angstrom exponent (Bohren and Huffman, 1983). For MSC the values were calculated for the whole period considered here (ALL; June 2011–June 2013), as well as for fall (SON), winter (DJF), spring (MAM) and summer (JJA). Red and yellow colours in Fig. 4 stay for *all-data* (averaged over 24 h) and *FT-data* (averaged between 03:00 a.m.–09:00 a.m.), respectively. The percentage

ACPD
14, 3777–3814, 2014

values in each figure represent the relative difference between the medians calculated for *all-data* and *FT-data*, with positive values indicating lower *FT-data* medians. The six red and yellow rectangles within the blue areas on the right of each figure represent the range of variability of the medians presented by AND2011 calculated for mountain-top sites in the Western Hemisphere (W), Europe (EU) and Eastern Hemisphere (E). Horizontal red and yellow lines represent the ALL median values at MSC calculated for *all-data* and *FT-data*, respectively.

As reported in Fig. 4 the scattering (Fig. 4a) and the absorption (Fig. 4b) measured at MSC for the whole dataset (ALL; Fig. 4a) locate the MSC site in the medium/upper range of EU ranges. This is especially marked for scattering data. The NAF and SREG episodes affecting the WMB have the potential to increase the aerosols mass and scattering measured in this area in summer (Fig. 3 and JJA scattering in Fig. 4a). Moreover, the high solar radiation in the Mediterranean Basin (especially in summer) favours the development of up-slope winds which, together with the possible presence of polluted residual layers at MSC altitude, contribute to the levels of scattering and absorption measured at MSC. Recently, Ripoll et al. (2013) have shown that the MSC site registers higher PM_{10} concentrations than those measured at other high-altitude central European sites and similar or lower BC concentrations. As a consequence, the SSA at MSC was relatively higher compared with the EU, W and E ranges of variability (Fig. 4d). Conversely, SAE and B/S were in the middle of the corresponding EU ranges.

All the extensive aerosol properties (scattering, absorption and extinction) showed relatively lower *FT-data* medians compared with *all-data* (16–19 %; ALL in Fig. 4a–c). This was a common characteristic for most of the stations presented in AND2011. However, the relative decreases in *FT-data* extensive properties were clearly a function of seasons at MSC site with the highest *FT* vs. *all-data* difference observed in winter (DJF in Fig. 4a–c; 21–23 %) and the lowest in spring/summer (MAM and JJA in Fig. 4a–c; 0–8 %). As a consequence of the time of day segregation used for the identification of FT air (3 a.m.–9 a.m. vs. 24 h) the remote sites with stronger DC tend to have

ACPD
14, 3777–3814, 2014

larger decreases in *FT* aerosol loading compared to *all-data* (24 h) aerosol loading (Andrews et al., 2011). Figure 5 shows that the strongest DC for scattering at MSC was observed in winter, whereas in spring and summer no clear DC was observed. The remarkable DC of aerosol scattering in winter was due to the position of MSC station in a mostly clean free troposphere at night, whereas the thermally-driven flows can transport pollutants toward MSC during the warmest hours of the day. In AND2011 all the low latitude sites ($< 30^{\circ}$ N) showed stronger diurnal cycles during all seasons compared with high latitude sites due to stronger insolation. The observed reduced DC for scattering at MSC during spring and summer was due to the occurrence of NAF and SREG episodes and wildfires in the WMB, together with the possible presence of intense polluted residual layers at night at the MSC altitude. These scenarios also linked with the high concentrations of PM and BC during the whole day as observed by Ripoll et al. (2013).

3.4 Relationships between σ_{sp} and other extensive/intensive aerosol properties

Figure 6 shows the relationships between σ_{sp} and some of the measured extensive (backscattering, absorption, PM_1 concentrations) and intensive (g, SAE, SSA) aerosol properties. Similar relationships were investigated e.g. by Delene and Ogren (2002), Pandolfi et al. (2011) and Andrews et al. (2011). This kind of relationships helps to constrain model parameterizations and to reduce uncertainties in the algorithms used for deriving intensive aerosol properties from remotely sensed data (Delene and Ogren, 2002).

As expected backscattering and PM_1 concentrations increased with increasing σ_{sp}. If the PM_1 concentrations increase the intensity of light scattered, and also backscattered, increases almost monotonically. Also the absorption, which is roughly proportional to the concentrations of absorbing aerosols in PM samples, increased with increasing scattering and PM_1 concentration. Similar findings were reported by Pandolfi et al. (2011) for the MSY RB site and by AND2011 (Fig. 6a in AND2011) for the 12 stations considered in their work. AND2011 observed that the measurement sites which

ACPD
14, 3777–3814, 2014

were dominated by dust aerosol at high aerosol loading tend to have a lower slope of the scattering–absorption relationship than the other sites. This is the case of MSC site showing a scattering–absorption slope in the lower range of those reported by AND2011 (cf. with Fig. 6a in AND2011).

The parameters g and SAE measured at MSC showed inverse relationships with σ_{sp}: when σ_{sp} increased above around 45–50 Mm^{-1} SAE decreased indicating the shift toward larger particles with relatively higher g and SSA. Figure 3 shows that these conditions (high scattering, low SAE and high SSA) were mainly associated with NAF scenarios with larger scattering particles. To further investigate this, Fig. 7 shows the distribution of σ_{sp} as a function of SAE by atmospheric scenarios (Fig. 7a) and by levels of PM_1/PM_{10} ratio (Fig. 7b).

As shown in Fig. 7a high scattering and relatively low SAE (< 1) were associated with NAF episodes (yellow colour). Correspondingly, the PM_1/PM_{10} ratio was among the lowest (0.2–0.3; Fig. 7b) indicating the prevalence of coarser particles. The ATL scenarios (blue colour in Fig. 7a) were mainly associated with relatively lower scattering, a broad range of SAE values (from −2 to 6) and PM_1/PM_{10} ratios around 0.3–0.5. Cermac et al. (2010) suggested that negative SAE could be an indication of reduced anthropogenic emissions with prevalence of coarse-mode particles. For example negative SAE and high Aerosol Optical Depth (AOD) have been related with transport of coarse-mode dust in northern India by Singh et al. (2004). However, extremely negative values of SAE are unfeasible for atmospheric aerosols. Similarly, the SAE cannot be higher than about 4 which represent the limit given by the Rayleigh regimen for the molecular scattering. In the present case 123 hourly values of SAE out of 9561 were smaller than −1 (1.2 %) and 150 values were higher than 4 (1.6 %). Consequently, the measured negative SAE at MSC were likely due to both the presence of relatively larger particles during low aerosol concentration (Fig. 7b) and the instrumental noise under low scattering conditions. Similar behaviour of SAE was also observed in a remote subartic site by Aaltonen et al. (2006) and at the MSY RB station by Pandolfi et al. (2011). Finally, the SREG episodes mainly (red colours; Fig. 7a), and to a lesser

ACPD
14, 3777–3814, 2014

extent WREG (orange colour), were associated with relatively larger SAE compared with NAF and high PM_1/PM_{10} ratios indicative of the prevalence of mainly fine particles of anthropogenic origin.

For σ_{sp} between around 20–40 Mm^{-1} (Fig. 6) both g and SAE showed relatively constant values around 0.55 (g) and 1.65 (SAE) which were close to the averages reported in Table 2 for these two parameters. When σ_{sp} was below around 20 Mm^{-1} SAE decreased indicating again the shift toward relatively larger particles associated with relatively clean atmosphere ($PM_1 < 5\,\mu g\,m^{-1}$). However, under very low PM_1 concentrations at MSC ($PM_1 < 1.5\,\mu g\,m^{-3}$) SSA and g reached very low values around 0.84 and 0.43, respectively, whereas the SAE increased (reaching around 1.6). Thus, these low PM conditions at MSC were associated with the prevalence of small particles with relatively higher absorption properties. Low values of SSA at very low aerosol loading have been observed in AND2011 and associated with an aerosol mixture in which large scattering aerosol particles have been preferentially removed (e.g., by cloud scavenging and/or deposition), leaving behind a relatively smaller and darker aerosol (e.g., AND2011; Berkowitz et al., 2011; Marcq et al., 2010; Targino et al., 2005; Sellegri et al., 2003).

3.5 MAC climatology

Mean MAC at MSC determined as the error-weighted slope of the absorption-EC concentration scatterplot was $11.1 \pm 0.3\,m^2\,g^{-1}$ ($R^2 = 0.82$). Given that σ_{ap} and EC measurements were available since the end of 2009, the mean MACs presented here were calculated over the period November 2009–June 2013 (406 sample pairs on 24 h base). On average lower MAC values were observed during AA ($9.7 \pm 0.7\,m^2\,g^{-1}$; $R^2 = 0.77$) and WREG ($9.4 \pm 1.0\,m^2\,g^{-1}$; $R^2 = 0.88$) scenarios compared to NAF ($11.9 \pm 0.7\,m^2\,g^{-1}$; $R^2 = 0.61$) and SREG ($12.6 \pm 1.0\,m^2\,g^{-1}$; $R^2 = 0.74$) scenarios. The non-parametric Kruskal–Wallis test was used for testing the equality of medians among the four selected categories (scenarios). Highly statistically significant differences ($p < 0.001$) were observed between the medians calculated during NAF and SREG,

ACPD
14, 3777–3814, 2014

compared with those obtained for AA and WREG. Conversely, no statistically significant differences were observed between WREG and AA ($p > 0.7$) and between NAF and SREG ($p > 0.4$). The higher MAC under NAF and SREG was likely due to the mixing of BC particles with other chemical components, such as sulphate and organics, which have the potential to increase the absorption properties of BC particles (e.g. Bond et al., 2013). As already stated, SREG is defined as a summer polluted scenario and the NAF episodes are more frequent in summer than in winter in the WMB. Many publications have shown higher sulphate (e.g. Pey et al., 2009) and organic matter concentrations (e.g. Querol et al., 2013) in summer compared to winter in the WMB at regional and remote levels. Moreover, recently Rodríguez et al. (2011) and Ripoll et al. (2013) have shown that pollutants such as sulphate and BC may be transported together with dust across the WMB during NAF episodes. Similar dependence of the MAC with atmospheric scenarios was observed by Pandolfi et al. (2011) at the RB Montseny station. As a consequence of the observed variation in the MAC values as a function of the four considered season-dependent scenarios, the MAC at MSC showed a clear annual cycle with the lowest values observed in winter and the highest in summer (Fig. 8). On average, also the pollutants transported toward the MSC station by the up-slope winds and PBL oscillations, which are expected to be more intense in summer, contributed to the observed MAC annual cycle. Similar seasonal dependence of the MAC with higher values in summer was observed at the Jungfraujoch high alpine site (Cozic et al., 2008).

4 Conclusions

The measurements of aerosol optical properties presented in this work and performed at Montsec remote site (MSC; 42°3′ N, 0°44′ E, 1570 m a.s.l.) add useful information on the rather little amount of in-situ aerosol optical data obtained at high altitude/mountaintop sites worldwide. The aerosol scattering measurements performed at MSC locate this site in the medium/upper range of values reported for other moun-

ACPD
14, 3777–3814, 2014

taintop sites in Europe (EU). The frequent African dust (NAF) outbreaks and regional recirculation (SREG) scenarios, typical of the WMB in spring/summer, together with the strong insolation favouring the development of up-slope winds, were mainly responsible for these relatively high values. The mean scattering at MSC under NAF and SREG scenarios were close to the values measured at a regional background station (Montseny; 720 m a.s.l.) thus demonstrating the potential of these two atmospheric scenarios in polluting the whole lower troposphere in the WMB. As a consequence, the strongest diurnal cycle (DC) for scattering at MSC was observed in winter, whereas in spring and summer no clear DC was observed due to the presence of polluted layer at the MSC altitude. Thus, the diurnal variation of scattering at MSC during spring and summer is subject to synoptic circulation which can mask the mountain breezes and the dynamics transport at a more local scale. Absorption at MSC was not as high as scattering compared with most of measurements in EU thus leading to relatively higher single scattering albedo (SSA) compared with EU data. Conversely, the scattering Angstrom exponent (SAE) and backscatter-to-scatter ratios (B/S) were on the middle of the corresponding EU ranges. Under Atlantic advection (AA) scenarios the lowest scattering and absorption were measured at MSC due to renovation of accumulated pollution in the aged air masses typically associated with AA episodes in the WMB.

All the extensive aerosol properties measured at MSC (scattering, absorption and extinction) showed relatively lower medians when MSC was in the free troposphere (*FT-data*) compared with the whole database (*all-data*). These decreases were clearly a function of seasons at MSC site with the highest *FT* vs. *all-data* difference observed in winter and the lowest in spring/summer.

The analysis of the relationships between scattering and other extensive/intensive aerosol properties measured at MSC showed a scattering–absorption slope in the lower range of slopes calculated worldwide indicating that the MSC site is dominated by dust aerosols at high aerosol loading. Under these conditions the SAE and asym-

ACPD
14, 3777–3814, 2014

metry parameter (g) respectively decreased and increased indicating the shift toward larger particles associated with NAF episodes.

The MAC estimated at MSC showed a clear annual cycle with higher values in summer when the occurrence of NAF and SREG scenarios favour the presence of polluted atmospheric layers containing aged BC particles likely mixed with other chemical components such as organics and sulfate.

Acknowledgements. This work is supported by the MINECO (Spanish Ministry of Economy and Competitiveness), the MAGRAMA (Spanish Ministry of Agriculture, Food Environment) and FEDER funds; the project PRISMA (CGL2012-39623-C02/00), VAMOS (CLG2010-19464). M. Pandolfi was funded by the JAE-Doc CSIC program, co-funded by the European Social Fund (ESF). The authors wish to thank D. C. Carslaw and K. Ropkins for providing the Openair software used in this paper (Carslaw and Ropkins, 2012; Carslaw, 2012). The authors gratefully acknowledge HYSPLIT model, SKIRON, BSC-DREAM and NRL-NAAPS aerosol maps, NCEP/NCAR meteorological database NOAA NAO index data, and image products from MODIS and SeaWiFs NASA satellites used in this publication.

References

Aaltonen, V., Lihavainen, H., Kerminen, V.-M., Komppula, M., Hatakka, J., Eneroth, K., Kulmala, M., and Viisanen, Y.: Measurements of optical properties of atmospheric aerosols in Northern Finland, Atmos. Chem. Phys., 6, 1155–1164, doi:10.5194/acp-6-1155-2006, 2006.

Anderson, T. L. and Ogren, J. A.: Determining aerosol radiative properties using the TSI 3563 integrating nephelometer, Aerosol Sci. Tech., 29, 57–69, 1998.

Andrews, E., Ogren, J. A., Sheridan, P. J., and Ferrare, R.: Vertical properties of aerosol optical properties at the ARM southern Great Plains CART site, J. Geophys. Res., 109, D06208, doi:10.1029/2003JD004025, 2004.

Andrews, E., Sheridan, P. J., Fiebig, M., McComiskey, A., Ogren, J. A., Arnott, P., Covert, D., Elleman, R., Gasparini, R., Collins, D., Jonsson, H., Schmid, B., and Wang, J.: Comparison of methods for deriving aerosol asymmetry parameter, J. Geophys. Res.-Atmos., 111, D05S04, doi:10.1029/2004JD005734, 2006.

ACPD
14, 3777–3814, 2014

Andrews, E., Ogren, J. A., Bonasoni, P., Marinoni, A., Cuevas, E., Rodríguez, S., Sun, J. Y., Jaffe, D. A., Fischer, E. V., Baltensperger, U., Weingartner, E., Collaud Coen, M., Sharma, S., Macdonald, A. M., Leaitch, W. R., Lin, N.-H., Laj, P., Arsov, T., Kalapov, I., Jefferson, A., and Sheridan, P.: Climatology of aerosol radiative properties in the free troposphere, Atmos. Res., 102, 365–393, doi:10.1016/j.atmosres.2011.08.017, 2011.

Arnott, W. P., Moosmüller, H., Sheridan, P. J., Ogren, J. A., Raspet, R., Slaton, W. V., Hand, J. L., Kreidenweis, S. M., and Collett Jr., J. L.: Photoacoustic and filter-based ambient aerosol light absorption measurements: instrument comparisons and the role of relative humidity, J. Geophys. Res., 108, 4034, doi:10.1029/2002JD002165, 2003.

Arnott, W. P., Hamasha, K., Moosmüller, H., Sheridan, P. J., and Ogren, J. A.: Towards aerosol light absorption measurements with a 7-wavelength aethalometer: evaluation with a photoacoustic instrument and 3 wavelength nephelometer, Aerosol Sci. Tech., 39, 17–29, 2005.

Berkowitz, C., Berg, L. K., Yu, X.-Y., Alexander, M. L., Laskin, A., Xie, Y., Jobson, B. T., Andrews, E., and Ogren, J.: A statistical overview of aerosol optical, chemical and physical measurements at a coastal northern California site during the summer of 2005, Atmos. Environ., 45, 2559–2568, doi:10.1016/j.atmosres.2011.08.017, 2011.

Bodhaine, B.: Aerosol measurements at four background sites, J. Geophys. Res., 88, 10753–10768, doi:10.1029/JC088iC15p10753, 1983.

Bodhaine, B.: Aerosol absorption measurements at Barrow, Mauna Loa and the South Pole, J. Geophys. Res., 100, 8967–8975, doi:10.1029/95JD00513, 1995.

Bohren, C. F. and Huffman, D. R.: Absorption and Scattering of Light by Small Particles, John Wiley and Sons, New York, 530 pp., 1983.

Bond, T. C. and Bergstrom, R. W.: Light absorption by carbonaceous particles: an investigative review, Aerosol Sci. Tech., 40, 27–67, doi:10.1080/02786820500421521, 2006.

Bond, T. C., Doherty, S. J., Fahey, D. W., Forster, P. M., Berntsen, T., DeAngelo, B. J., Flanner, M. G., Ghan, S., Kärcher, B., Koch, D., Kinne, S., Kondo, Y., Quinn, P. K., Sarofim, M. C., Schultz, M. G., Schulz, M., Venkataraman, C., Zhang, H., Zhang, S., Bellouin, N., Guttikunda, S. K., Hopke, P. K., Jacobson, M. Z., Kaiser, J. W., Klimont, Z., Lohmann, U., Schwarz, J. P., Shindell, D., Storelvmo, T., Warren, S. G., and Zender, C. S.: Bounding the role of black carbon in the climate system: a scientific assessment, J. Geophys. Res., 118, 5380–5552, doi:10.1002/jgrd.50171, 2013.

Carslaw, D. C.: The Openair Manual – Open-Source Tools for Analysing Air Pollution Data, Manual for version 0.7-0, King's College, London, 2012.

ACPD
14, 3777–3814, 2014

Carslaw, D. C. and Ropkins, K.: openair – an R package for air quality data analysis, Environ. Modell. Softw., 27–28, 52–61, 2012.
Cavalli, F., Viana, M., Yttri, K. E., Genberg, J., and Putaud, J.-P.: Toward a standardised thermal-optical protocol for measuring atmospheric organic and elemental carbon: the EUSAAR protocol, Atmos. Meas. Tech., 3, 79–89, doi:10.5194/amt-3-79-2010, 2010.
Cermak, J., Wild, M., Knutti, R., Mishchenko, M. I., and Heidinger, A. K.: Consistency of global satellite-derived aerosol and cloud data sets with recent brightening observations, Geophys. Res. Lett., 37, L21704, doi:10.1029/2010gl044632, 2010.
Collaud Coen, M., Weingartner, E., Schaub, D., Hueglin, C., Corrigan, C., Henning, S., Schwikowski, M., and Baltensperger, U.: Saharan dust events at the Jungfraujoch: detection by wavelength dependence of the single scattering albedo and first climatology analysis, Atmos. Chem. Phys., 4, 2465–2480, doi:10.5194/acp-4-2465-2004, 2004.
Collaud Coen, M., Weingartner, E., Nyeki, S., Cozic, J., Henning, S., Verheggen, B., Gehrig, R., and Baltensperger, U.: Long-term trend analysis of aerosol variables at the high-alpine site Jungfraujoch, J. Geophys. Res., 112, D13213, doi:10.1029/2006JD007995, 2007.
Collaud Coen, M., Weingartner, E., Furger, M., Nyeki, S., Prévôt, A. S. H., Steinbacher, M., and Baltensperger, U.: Aerosol climatology and planetary boundary influence at the Jungfraujoch analyzed by synoptic weather types, Atmos. Chem. Phys., 11, 5931–5944, doi:10.5194/acp-11-5931-2011, 2011.
Cozic, J., Verheggen, B., Weingartner, E., Crosier, J., Bower, K. N., Flynn, M., Coe, H., Henning, S., Steinbacher, M., Henne, S., Collaud Coen, M., Petzold, A., and Baltensperger, U.: Chemical composition of free tropospheric aerosol for PM1 and coarse mode at the high alpine site Jungfraujoch, Atmos. Chem. Phys., 8, 407–423, doi:10.5194/acp-8-407-2008, 2008.
Delene, D. J. and Ogren, J. A.: Variability of aerosol optical properties at four North American surface monitoring sites, J. Atmos. Sci., 59, 1135–1150, 2002.
Fernández-Camacho, R., Rodríguez, S., de la Rosa, J., Sánchez de la Campa, A. M., Viana, M., Alastuey, A., and Querol, X.: Ultrafine particle formation in the inland sea breeze airflow in Southwest Europe, Atmos. Chem. Phys., 10, 9615–9630, doi:10.5194/acp-10-9615-2010, 2010.
Fierz-Schmidhauser, R., Zieger, P., Wehrle, G., Jefferson, A., Ogren, J. A., Baltensperger, U., and Weingartner, E.: Measurement of relative humidity dependent light scattering of aerosols, Atmos. Meas. Tech., 3, 39–50, doi:10.5194/amt-3-39-2010, 2010.

ACPD
14, 3777–3814, 2014

Gangoiti, G., Millán, M. M., Salvador, R., and Mantilla, E.: Long-Range transport and recirculation of pollutants in the Western Mediterranean during the project regional cycles of air pollution in the west-central Mediterranean Area, Atmos. Environ., 35, 6267–6276, 2001.

IPCC 2007: Climate Change 2007: The Physical Science Basis (Contribution of Working Group I to the Fourth Assessment Report of the Intergovernmental Panel on Climate Change), edited by: Solomon, S., Qin, D. Manning, M., Chen, Z., Marquis, M., Averyt, K. B., Tignor, M., and Miller, H. L., Cambridge Univ. Press, New York, USA, 131–217, 2007.

IPCC 2013: Climate Change 2013: The Physical Science Basis. Working Group I contribution to the IPCC fifth assessment report, Final Draft Underlying Scientific-Technical Assessment, Cambridge University Press, Cambridge, United Kingdom and New York, NY, USA, 2013.

Jorba, O., Pandolfi, M., Spada, M., Baldasano, J. M., Pey, J., Alastuey, A., Arnold, D., Sicard, M., Artinano, B., Revuelta, M. A., and Querol, X.: Meteorological overview and transport patterns of the DAURE field campaign: link to PM observations, Atmos. Environ., 77, 607–620, 2013.

JRC Report: Measurement of Elemental and Organic Carbon in Europe, Scientific and Technical Reports, EUR 23922 EN-2009, Joint Research Center, Ispra, Italy, 2009.

Laj, P., Klausen, J., Bilde, M., Plaß-Duelmer, C., Pappalardo, G., Clerbaux, C., Baltensperger, U., Hjorth, J., Simpson, D., Reimann, S., Coheur, P.-F., Richter, A., De Mazière, M., Rudich, Y., McFiggans, G., Torseth, K., Wiedensohler, A., Morin, S., Schulz, M., Allan, J. D., Attié, J.-L., Barnes, I., Birmili, W., Cammas, J. P., Dommen, J., Dorn, H.-P., Fowler, D., Fuzzi, S., Glasius, M., Granier, C., Hermann, M., Isaksen, I. S. A., Kinne, S., Koren, I., Madonna, F., Maione, M., Massling, A., Moehler, O., Mona, L., Monks, P. S., Müller, D., Müller, T., Orphal, J., Peuch, V.-H., Stratmann, F., Tanré, D., Tyndall, G., Abo Riziq, A., Van Roozendael, M., Villani, P., Wehner, B., Wex, H., and Zardini, A. A.: Measuring atmospheric composition change, Atmos. Environ., 43, 5351–5414, doi:10.1016/j.atmosenv.2009.08.020, 2009.

Marinoni, A., Cristofanelli, P., Calzolari, F., Roccato, F., Bonafe, U., and Bonasoni, P.: Continuous measurements of aerosol physical parameters at the Mt. Cimone GAW station (2165 m a.s.l., Italy), Sci. Total. Environ., 391, 241–251, 2008.

Marcq, S., Laj, P., Roger, J. C., Villani, P., Sellegri, K., Bonasoni, P., Marinoni, A., Cristofanelli, P., Verza, G. P., and Bergin, M.: Aerosol optical properties and radiative forcing in the high Himalaya based on measurements at the Nepal Climate Observatory-Pyramid site (5079 m a.s.l.), Atmos. Chem. Phys., 10, 5859–5872, doi:10.5194/acp-10-5859-2010, 2010.

ACPD
14, 3777–3814, 2014

McKendry, I., Strawbridge, K., Karumudi, M. L., O'Neill, N., Macdonald, A. M., Leaitch, R., Jaffe, D., Cottle, P., Sharma, S., Sheridan, P., and Ogren, J.: Californian forest fire plumes over Southwestern British Columbia: lidar, sunphotometry, and mountaintop chemistry observations, Atmos. Chem. Phys., 11, 465–477, doi:10.5194/acp-11-465-2011, 2011.

Millán, M. M., Artiñano, B., Alonso, L., Castro, M., Fernández-Patier, R., and Goberna, J.: Mesometeorological Cycles of Air Pollution in the Iberian Peninsula, (MECAPIP), Contract EV4V-0097-E, Air Pollution Research Report 44, (Eur No. 14834) CEC-DG XII/E-1, Rue de la Loi, 200, 1040, Bruselas, 219 pp., 1992.

Millán, M. M., Salvador, R., Mantilla, E., and Kallos, G.: Photooxidant dynamics in the Mediterranean basin in summer: results from European research projects, J. Geophys. Res., 102, 8811–8823, doi:10.1029/96JD03610, 1997.

Müller, T., Laborde, M., Kassell, G., and Wiedensohler, A.: Design and performance of a three-wavelength LED-based total scatter and backscatter integrating nephelometer, Atmos. Meas. Tech., 4, 1291–1303, doi:10.5194/amt-4-1291-2011, 2011a.

Müller, T., Henzing, J. S., de Leeuw, G., Wiedensohler, A., Alastuey, A., Angelov, H., Bizjak, M., Collaud Coen, M., Engström, J. E., Gruening, C., Hillamo, R., Hoffer, A., Imre, K., Ivanow, P., Jennings, G., Sun, J. Y., Kalivitis, N., Karlsson, H., Komppula, M., Laj, P., Li, S.-M., Lunder, C., Marinoni, A., Martins dos Santos, S., Moerman, M., Nowak, A., Ogren, J. A., Petzold, A., Pichon, J. M., Rodriquez, S., Sharma, S., Sheridan, P. J., Teinilä, K., Tuch, T., Viana, M., Virkkula, A., Weingartner, E., Wilhelm, R., and Wang, Y. Q.: Characterization and intercomparison of aerosol absorption photometers: result of two intercomparison workshops, Atmos. Meas. Tech., 4, 245–268, doi:10.5194/amt-4-245-2011, 2011b.

Nyeki, S., Baltensperger, U., Colbeck, I., Jost, D. T., Weingartner, E., and Gaggeler, H. W.: The Jungfraujoch high-alpine research station (3454 m) as a background clean continental site for the measurement of aerosol parameters, J. Geophys. Res., 103, 6097–6107, doi:10.1029/97JD03123, 1998.

Ogren, J. A., Andrews, E., McComiskey, A., Sheridan, P., Jefferson, A., and Fiebig, M.: New insights into aerosol asymmetry parameter, in: Proceedings of the 16th ARM Science Team Meeting, Albuquerque, NM, USA, 2006.

Pandolfi, M., Cusack, M., Alastuey, A., and Querol, X.: Variability of aerosol optical properties in the Western Mediterranean Basin, Atmos. Chem. Phys., 11, 8189–8203, doi:10.5194/acp-11-8189-2011, 2011.

ACPD
14, 3777–3814, 2014

Pereira, S. N., Wagner, F., and Silva, A. M.: Seven years of measurements of aerosol scattering properties, near the surface, in the southwestern Iberia Peninsula, Atmos. Chem. Phys., 11, 17–29, doi:10.5194/acp-11-17-2011, 2011.

Pérez, C., Sicard, M., Jorba, O., Comerón, A., and Baldasano, J. M.: Summertime recirculations of air pollutants over the northeastern Iberian coast observed from systematic EARLINET lidar measurements in Barcelona, Atmos. Environ., 38, 3983–4000, doi:10.1016/j.atmosenv.2004.04.010, 2004.

Pérez, N., Pey, J., Castillo, S., Viana, M., Alastuey, A., and Querol, X.: Interpretation of the variability of levels of regional background aerosols in the Western Mediterranean, Sci. Total Environ., 407, 527–540, doi:10.1016/j.scitotenv.2008.09.006, 2008.

Petzold, A. and Schönlinner, M.: Multi-angle absorption photometry – a new method for the measurement of aerosol light absorption and atmospheric black carbon, J. Aerosol Sci., 35, 421–441, doi:10.1016/j.jaerosci.2003.09.005, 2004.

Pey, J., Pérez, N., Castillo, S., Viana, M., Moreno, T., Pandolfi, M., López-Sebastián, J. M., Alastuey, A., and Querol, X.: Geochemistry of regional background aerosols in the Western Mediterranean, Atmos. Res., 94, 422–435, doi:10.1016/j.atmosres.2009.07.001, 2009.

Pey, J., Querol, X., Alastuey, A., Forastiere, F., and Stafoggia, M.: African dust outbreaks over the Mediterranean Basin during 2001–2011: PM_{10} concentrations, phenomenology and trends, and its relation with synoptic and mesoscale meteorology, Atmos. Chem. Phys., 13, 1395–1410, doi:10.5194/acp-13-1395-2013, 2013.

Polissar, A. V., Hopke, P. K., Malm, W. C., and Sisler, J. F.: Atmospheric aerosols over Alaska: 2. Elemental composition and sources, J. Geophys. Res., 103, 19045–19057, doi:10.1029/98JD01212, 1998.

Quinn, P. K. and Bates, T. S.: Regional aerosol properties: comparisons of boundary layer measurements from ACE 1, ACE 2, Aerosols99, INDOEX, ACE Asia, TARFOX, and NEAQS, J. Geophys. Res., 110, D14202, doi:10.1029/2004JD004755, 2005.

Querol, X., Pey, J., Minguillón, M. C., Pérez, N., Alastuey, A., Viana, M., Moreno, T., Bernabé, R. M., Blanco, S., Cárdenas, B., Vega, E., Sosa, G., Escalona, S., Ruiz, H., and Artíñano, B.: PM speciation and sources in Mexico during the MILAGRO-2006 Campaign, Atmos. Chem. Phys., 8, 111–128, doi:10.5194/acp-8-111-2008, 2008.

Querol, X., Alastuey, A., Pey, J., Cusack, M., Pérez, N., Mihalopoulos, N., Theodosi, C., Gerasopoulos, E., Kubilay, N., and Koçak, M.: Variability in regional background aerosols

ACPD
14, 3777–3814, 2014

within the Mediterranean, Atmos. Chem. Phys., 9, 4575–4591, doi:10.5194/acp-9-4575-2009, 2009.

Querol, X., Alastuey, A., Viana, M., Moreno, T., Reche, C., Minguillón, M. C., Ripoll, A., Pandolfi, M., Amato, F., Karanasiou, A., Pérez, N., Pey, J., Cusack, M., Vázquez, R., Plana, F., Dall'Osto, M., de la Rosa, J., Sánchez de la Campa, A., Fernández-Camacho, R., Rodríguez, S., Pio, C., Alados-Arboledas, L., Titos, G., Artíñano, B., Salvador, P., García Dos Santos, S., and Fernández Patier, R.: Variability of carbonaceous aerosols in remote, rural, urban and industrial environments in Spain: implications for air quality policy, Atmos. Chem. Phys., 13, 6185–6206, doi:10.5194/acp-13-6185-2013, 2013.

Reche, C., Querol, X., Alastuey, A., Viana, M., Pey, J., Moreno, T., Rodríguez, S., González, Y., Fernández-Camacho, R., de la Rosa, J., Dall'Osto, M., Prévôt, A. S. H., Hueglin, C., Harrison, R. M., and Quincey, P.: New considerations for PM, Black Carbon and particle number concentration for air quality monitoring across different European cities, Atmos. Chem. Phys., 11, 6207–6227, doi:10.5194/acp-11-6207-2011, 2011.

Ripoll, A., Pey, J., Minguillón, M. C., Pérez, N., Pandolfi, M., Querol, X., and Alastuey, A.: Three years of aerosol mass, black carbon and particle number concentrations at Montsec (southern Pyrenees, 1570 m a.s.l.), Atmos. Chem. Phys. Discuss., 13, 27201–27241, doi:10.5194/acpd-13-27201-2013, 2013.

Rodríguez, S., Querol, X., Alastuey, A., Kallos, G., and Kakaliagou, O.: Saharan dust contributions to PM_{10} and TSP levels in Southern and Eastern Spain, Atmos. Environ., 35, 2433–2447, doi:10.1016/S1352-2310(00)00496-9, 2001.

Rodríguez, S., Querol, X., Alastuey, A., Viana, M. M., Alarcón, M., Mantilla, E., and Ruiz, C. R.: Comparative PM_{10}–$PM_{2.5}$ source contribution study at rural, urban and industrial sites during PM episodes in Eastern Spain, Sci. Total. Environ., 26, 328, 95–113, doi:10.1016/S0048-9697(03)00411-X, 2004.

Rodríguez, S., Alastuey, A., Alonso-Pérez, S., Querol, X., Cuevas, E., Abreu-Afonso, J., Viana, M., Pérez, N., Pandolfi, M., and de la Rosa, J.: Transport of desert dust mixed with North African industrial pollutants in the subtropical Saharan Air Layer, Atmos. Chem. Phys., 11, 6663–6685, doi:10.5194/acp-11-6663-2011, 2011.

Schuster, G. L., Dubovik, O., and Holben, B. N.: Ångström exponent and bimodal aerosol size distributions, J. Geophys. Res., 111, D07207, doi:10.1029/2005JD006328, 2006.

ACPD
14, 3777–3814, 2014

Sellegri, K., Laj, P., Dupuy, R., Legrand, M., Preunkert, S., and Putaud, J.-P.: Size-dependent scavenging efficiencies of multicomponent atmospheric aerosols in clouds, J. Geophys. Res., 108, 4334, doi:10.1029/2002JD002749, 2003.

Singh, R. P., Dey, S., Tripathi, S. N., Tare, V., and Holben, B. N.: Variability of aerosol parameters over Kanpur city, northern India, J. Geophys. Res., 109, D23206, doi:10.1029/2004JD004966, 2004.

Targino, A. C., Noone, K. J., and Ostrom, E.: Airborne in-situ characterization of dry aerosol optical properties in a multisource influenced marine region, Tellus B, 57, 247–260, doi:10.1111/j.1600-0889.2005.00147.x, 2005.

ACPD
14, 3777–3814, 2014

Table 1. Significance of acronyms used in this work.

Acronyms	
Extensive aerosol optical properties	
σ_{sp}:	particle scattering
σ_{bsp}:	particle backscattering
σ_{ap}:	particle absorption
Intensive aerosol optical properties	
SSA:	single scattering albedo
SAE:	scattering Ångström exponent
B/S:	backscatter-to-scatter ratio
g:	asymmetry parameter
MAC:	mass absorption cross section
Concentration measurements	
BC:	black carbon
EC:	elemental carbon
PM_1:	particles with aerodynamic diameter < 1 µm
PM_{10}:	particles with aerodynamic diameter < 10 µm
Measurement sites	
MSC:	Montsec
MSY:	Montseny
Air masses	
AA:	Atlantic Ocean Advections
NAF:	North Africa
WAE:	winter-regional scenario
SREG:	summer-regional scenario
Others	
WMB:	Western Mediterranean Basin
PBL:	Planetary Boundary Layer
FT:	Free troposphere
RB:	Regional background

ACPD
14, 3777–3814, 2014

Table 2. Statistics of the considered aerosol components and parameters for the period June 2011–June 2013 at Montsec site (*all data*). The wavelength (λ) is given in [nm]; Scattering (σ_{sp}), backscattering (σ_{bsp}) and absorption coefficients (σ_{ap}) are given in [Mm^{-1}]; Backscattering-to-scattering ratio (B/S), asymmetry parameter (g), single scattering albedo (SSA) and Ångström exponent (SAE) are dimensionless; PM_1 concentrations are given in [$\mu g\,m^{-3}$]; MAC is expressed in [$m^2\,g^{-1}$]. Statistics based on hourly mean values (24 h for MAC). Optical data were referenced to STP ($T_{standard}$ = 273.15 K and $P_{standard}$ = 1013.25 hPa).

Hourly base	λ	counts	mean	SD	Median (50th perc.)	min	max	skewness	percentiles 1	10	25	75	99
σ_{sp}	635	10 014	18.9	20.8	11.2	0.1	161.1	1.83	0.2	1.1	3.5	28.3	89.8
	525	10 014	25.4	27.5	15.1	0.1	222.2	1.68	0.1	1.6	4.5	38.6	118.5
	450	10 014	32.3	34.7	19.3	0.1	276.2	1.62	0.1	2.0	5.6	49.6	143.6
σ_{bsp}	635	10 014	2.6	2.8	1.7	0.0	17.1	1.25	0.1	0.2	0.4	4.3	11.1
	525	10 014	3.1	3.2	1.9	0.0	36.4	1.31	0.1	0.2	0.5	5.1	12.8
	450	10 014	3.6	3.9	2.2	0.0	96.0	1.21	0.1	0.2	0.5	6.0	14.6
B/S	635	8612	0.16	0.09	0.15	0.02	0.99	4.03	0.04	0.10	0.12	0.18	0.58
	525	8864	0.13	0.07	0.13	0.01	0.98	4.78	0.04	0.09	0.11	0.15	0.44
	450	8761	0.12	0.06	0.11	0.01	1.00	4.95	0.03	0.07	0.10	0.13	0.36
σ_{ap}	637	13 712	1.5	1.4	1.0	0.0	12.6	1.45	0.0	0.1	0.3	2.4	6.2
g	635	8587	0.53	0.16	0.54	−0.99	0.93	−2.51	−0.10	0.39	0.49	0.60	0.85
	525	8858	0.59	0.13	0.59	−0.92	0.94	−3.25	0.09	0.49	0.55	0.64	0.85
	450	8755	0.62	0.11	0.62	−0.79	0.95	−2.15	0.20	0.53	0.58	0.66	0.88
SAE	450–635	9561	1.56	0.88	1.65	−1.96	5.99	0.30	−1.14	0.56	1.22	1.90	4.69
SSA	635	6123	0.92	0.03	0.93	0.45	0.99	−2.59	0.81	0.89	0.91	0.94	0.97
MAC	637	384	10.9	3.5	11.1	2.4	20.8	0.21	3.6	6.2	8.2	13.2	19.8
PM_1	–	10 949	5.3	4.5	4.0	0.1	49.9	2.06	0.5	1.4	1.9	7.2	21.8

ACPD
14, 3777–3814, 2014

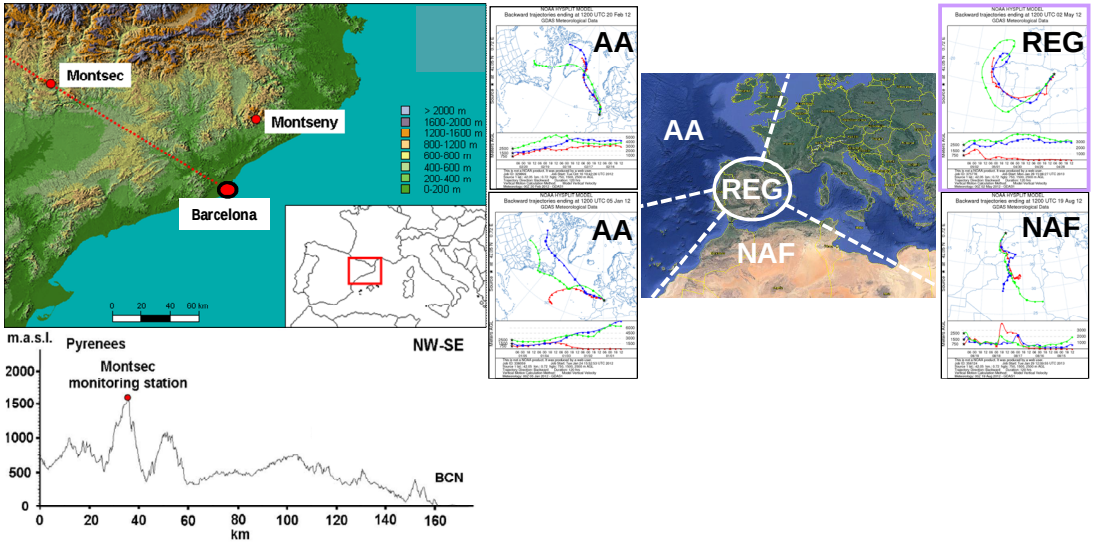

Fig. 1. Location of the Montsec (MSC; remote-mountaintop site) and Montseny (MSY; regional background (RB)) measurement sites. Air mass backtrajectories from Atlantic Ocean (AA), regional (REG) and North Africa (NAF).

ACPD
14, 3777–3814, 2014

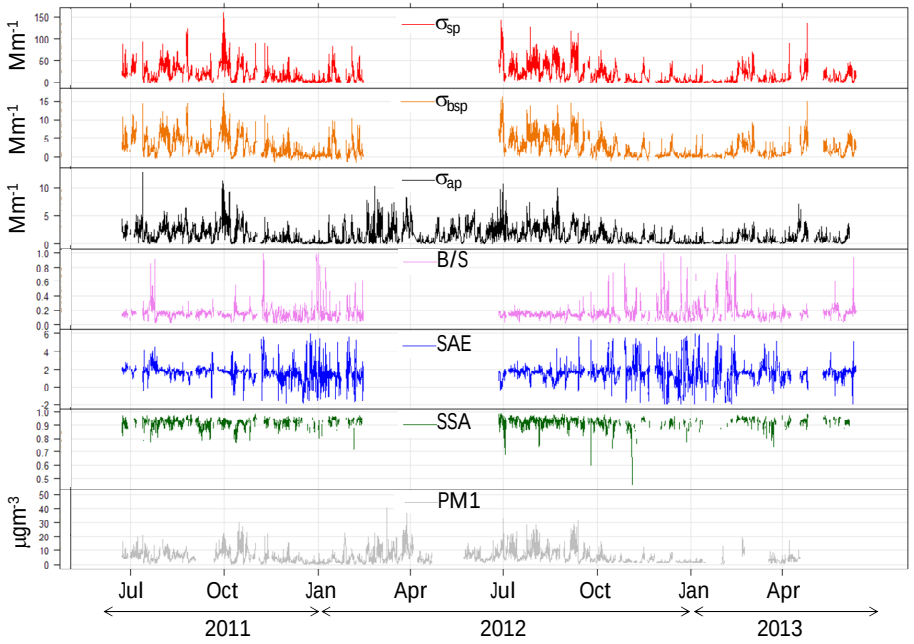

Fig. 2. Temporal series of scattering (σ_{sp}) and backscattering (σ_{bsp}) coefficients at 635 nm, absorption coefficient (σ_{ap}) at 637 nm, backscatter-to-scatter ratio (B/S) at 635 nm, scattering Ångström exponent (SAE) between 450 and 635 nm, single scattering albedo (SSA) at 635 nm, and PM_1 concentrations.

ACPD
14, 3777–3814, 2014

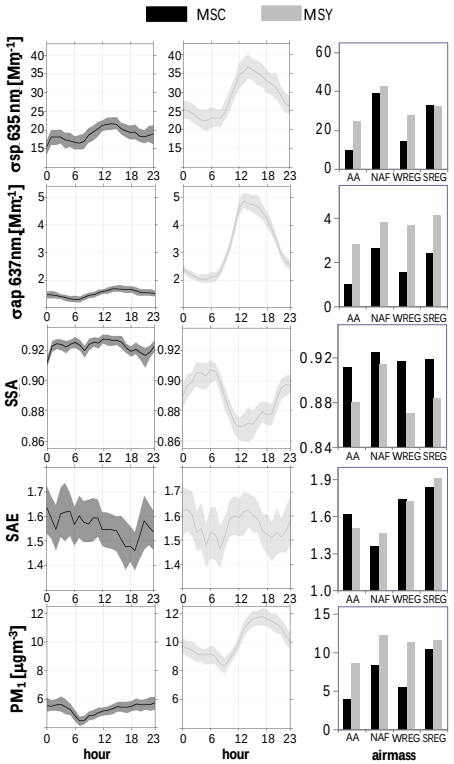

Fig. 3. Diurnal cycles and cluster analysis of scattering (σ_{sp} at 635 nm), absorption (σ_{ap} at 637 nm), single scattering albedo (SSA at 635 nm), scattering Ångström exponent (SAE calculated between 450 and 635 nm) and PM_1 concentrations measured at Montsec site (MSC; black lines) and at Montseny RB site (MSY; grey lines). Atmospheric scenarios are: Atlantic advection (AA), African dust outbreaks (NAF), winter regional anticyclonic episodes (WREG) and summer regional recirculation episodes (SREG).

ACPD
14, 3777–3814, 2014

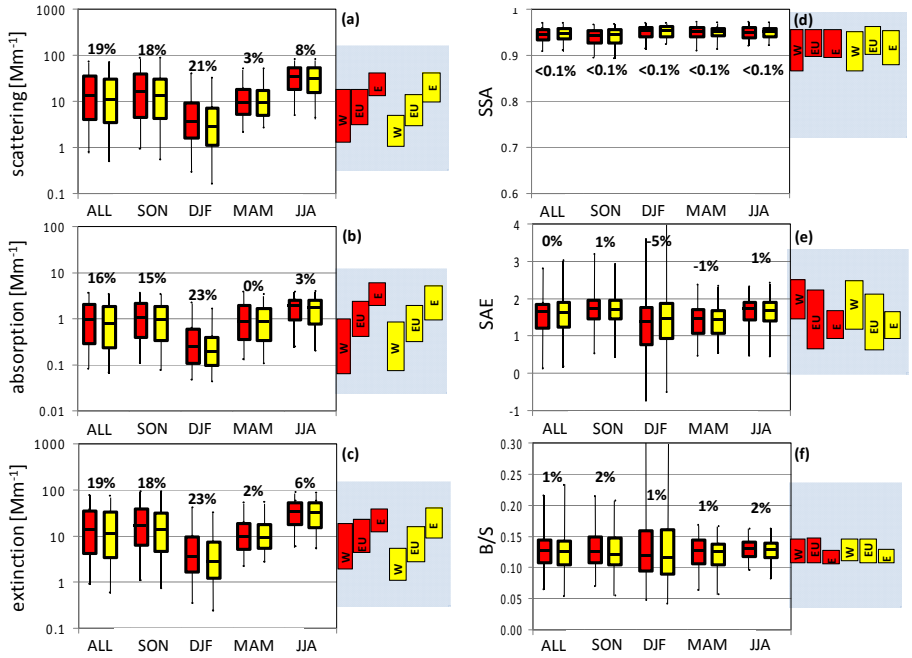

Fig. 4. Aerosol optical properties for *all-data* and *FT-data* data. Data are reported at 550 nm. Red = *all-data*, Yellow = *FT-data*. Horizontal lines within the boxes are the medians (50th percentile), edges of box are 25th and 75th percentiles, and whiskers are 5th and 95th percentiles. Ångström exponent is calculated for 450/635 nm pair. For MSC values are calculated for the whole period considered here (ALL), and for fall (SON), winter (DJF), spring (MAM) and summer (JJA). The percentage values represent the relative difference between the medians calculated for *all-data* and *FT-data*. The red and yellow rectangles within the blue areas on the right of each figure represent the range of variability of the medians presented by Andrews et al. (2011) calculated for sites in the Western Hemisphere (W), Europe (EU) and Eastern Hemisphere (E).

ACPD
14, 3777–3814, 2014

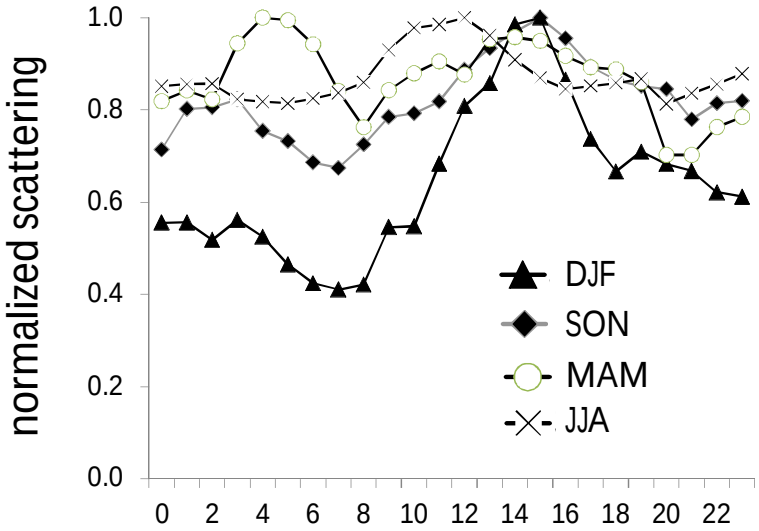

Fig. 5. Diurnal cycles of normalized aerosol scattering at 550 nm measured at MSC as a function of the seasons: winter (DJF), fall (SON), spring (MAM) and summer (JJA).

ACPD
14, 3777–3814, 2014

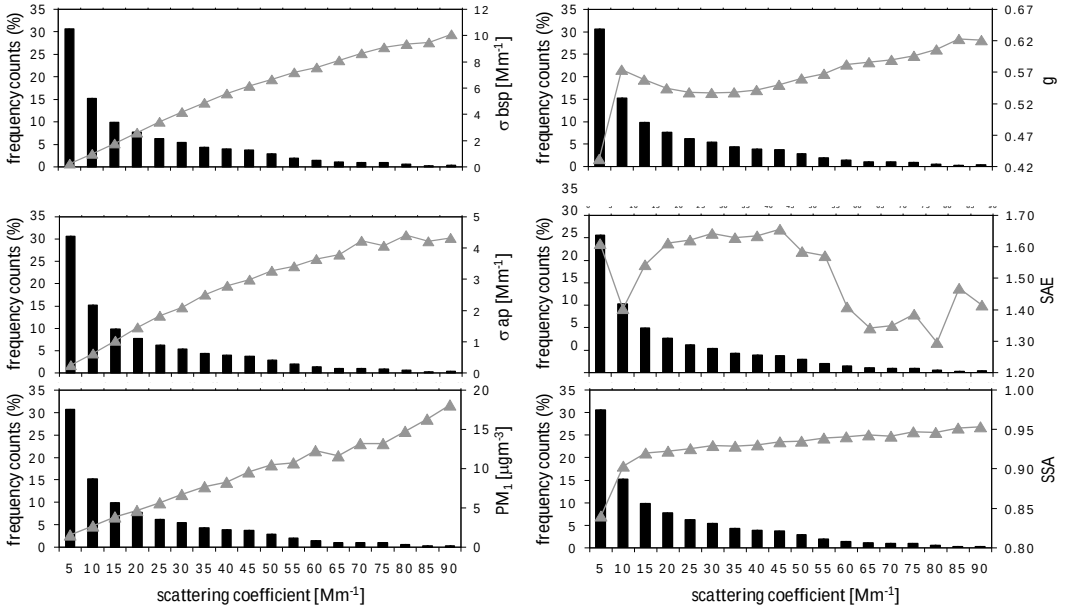

Fig. 6. Correlation between the frequency distribution of aerosol scattering coefficients (σ_{sp}) at 635 nm and backscattering coefficient (σ_{bsp} at 635 nm), absorption coefficient (σ_{ap} at 637 nm), PM_1 concentrations (PM_1), asymmetry parameter (g at 635 nm), scattering Ångström exponent (SAE; 450–635 nm), single scattering albedo (SSA at 635 nm).

ACPD
14, 3777–3814, 2014

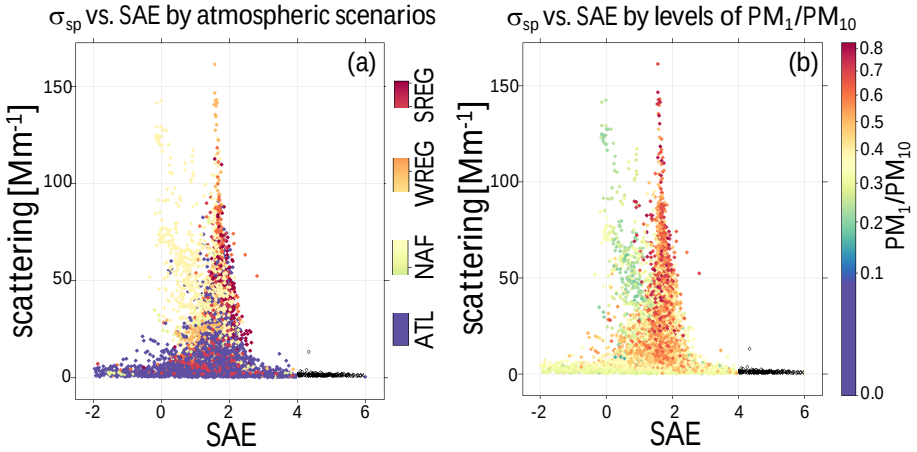

Fig. 7. Scattering coefficient (σ_{sp}) distribution at 635 nm as a function of scattering Ångström exponent (SAE) by atmospheric scenarios **(a)** and by levels of PM_1/PM_{10} ratio **(b)**. Dark data points indicate SAE > 4.

ACPD
14, 3777–3814, 2014

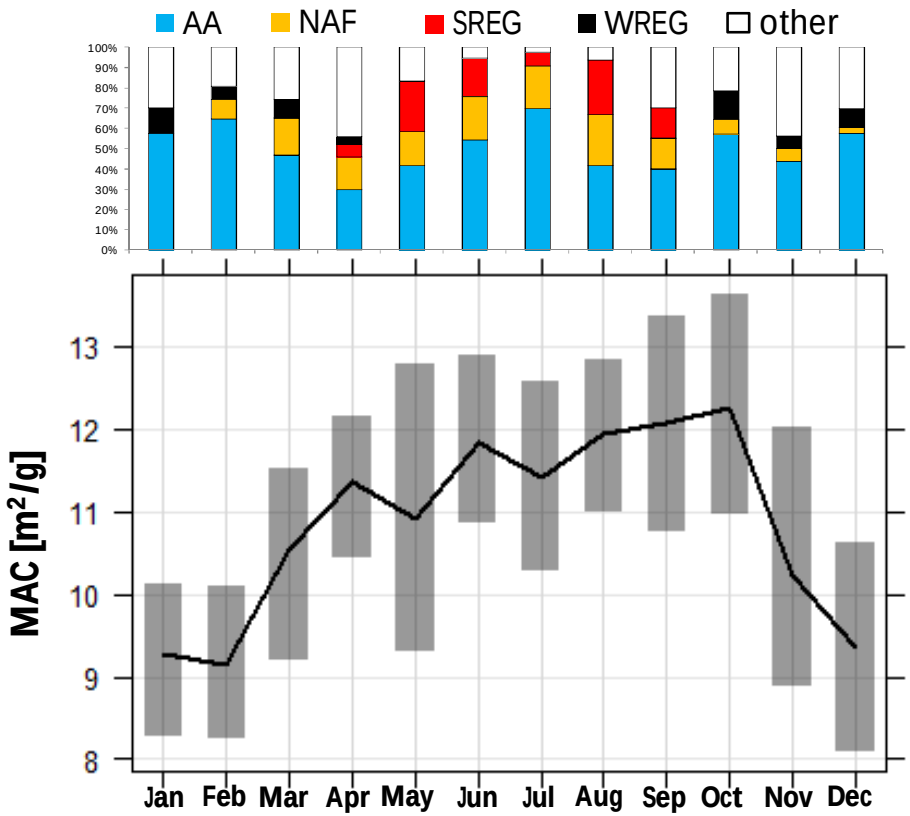

Fig. 8. Monthly mean MAC at MSC station and occurrence (%) of the main atmospheric scenarios (AA: Atlantic advections; NAF: Saharan dust outbreaks; SREG: summer regional recirculation scenarios; WREG: winter anticyclonic scenarios). Bars represent 95 % confidence intervals.

ACPD
14, 3777–3814, 2014